1-1-2016

Walker Design for Kinetic Assessment of Upper Extremity Joint Demands in Children with Osteogenesis Imperfecta

Katherine A. Konop
Orthopedic and Rehabilitation Engineering Center

Kelly M.B. Strifling
Orthopedic and Rehabilitation Engineering Center

Mei Wang
Marquette University, mei.wang@marquette.edu

Jeffrey P. Schwab
Orthopedic and Rehabilation Engineering Center

Jeffrey D. Ackman
Shriners Hospitals For Children

See next page for additional authors

Published version. *Transitional Care in Osteogenesis Imperfecta: Advances in biology, Technology, and Clinical Practice*, (2016): pp. 327-344. Publisher link.

19 WALKER DESIGN FOR KINETIC ASSESSMENT OF UPPER EXTREMITY JOINT DEMANDS IN CHILDREN WITH OSTEOGENESIS IMPERFECTA

Katherine A. Konop, M.S.[1]
Kelly M.B. Strifling, Ph.D.[1]
Mei Wang, Ph.D.[1]
Jeffrey P. Schwab, M.D.[1]
Jeffery D. Ackman, M.D.[2]
Peter A. Smith, M.D.[2]
Gerald F. Harris, P.E., Ph.D.[1,2]

[1] Orthopaedic and Rehabilitation Engineering Center (OREC),
Marquette University and The Medical College of Wisconsin, Milwaukee, WI
[2] Shriners Hospitals for Children, Chicago, IL

INTRODUCTION

Osteogenesis imperfecta (OI) is a congenital disease caused by a defect in the gene that produces type 1 collagen. One of the main effects is extremely fragile bones. OI affects 1 in 10,000 individuals in the United States.[1] There are eight types of OI, with type I being the most common and mildest form. Type II and type III are quite severe, while type IV is known as moderately severe OI. Type V and type VI are clinically similar to type IV, with histologic differences. Type VII is autosomal recessive and type VIII is very severe.

People with OI are encouraged to exercise as much as possible to promote muscle and bone strength. Walking is an excellent form of exercise for those with OI. Many children with various types of OI walk using mobility aids.[2]

Walking aids, such as walkers, crutches, or canes can allow a person to achieve weight bearing ambulation when their lower extremities (LEs) are not able to support the entire weight of their body. Walking aids allow some of the load to be distributed to the upper extremities (UEs). Since the UEs of bipeds are not accustomed to the magnitude and repetition of the loads

associated with gait, it is important to quantify the dynamic loads placed on them.

Motion analysis is an important biomechanical tool for evaluating the movement of body segments over time. Motion analysis is widely used to study LE gait, but has seen limited application to the UEs. Because of the range of UE activities studied, and lack of repeatable activity such as gait for the LEs, several types of UE kinematic models have been developed, and the results are not easily comparable. Work has been done by the International Society of Biomechanics to standardize UE models in terms of reference frames and reporting methods.[3]

This study will examine how the use of an instrumented walker, along with motion analysis, can provide information on the loads experienced by the UE joints during aided ambulation.

PREVIOUS WORK

Studies have been done to characterize forces internal to the walker structure (walker forces), where most examine walker leg loads and moments.[4–8] These methods do not allow for bilateral distinction of UE loading, and are insufficient for the determination of internal joint reaction forces and moments.

Our group developed an instrumented walker system that was able to detect contact forces and moments from the left and right hands separately. The initial design by Bachschmidt et al. included 24 resistive foil strain gages (six four-arm strain gage bridges) epoxied directly to each walker handle.[9,10] The strain gages were positioned in such a way to sense bending loads in the transverse and sagittal planes (sections AA and CC in Figure 1), as well as torsional and axial loads (section BB in Figure 1). Disadvantages of this system included potential for error in the mounting process and the inability to be applied easily to other devices.

A subsequent design was developed in conjunction with Advanced Medical Technology, Incorporated (AMTI). Custom dynamometers (model MCW-6-500, AMTI, Watertown, MA) that mounted to removable handle stems were created. They were 6-axis load cells, able to detect forces along three axes and moments about three axes, with a 500-pound capacity. The handle stems mounted to the walker with brackets allowing the height and angle to be

adjusted to the patients' needs. Positioning the load cells as close to the hands as possible minimized the cross-talk (less than 2%) from the statically indeterminate frame.[11] The non-linearity and hysteresis of the dynamometers were less than ±0.20%, and the lowest resonant frequency of a stand-alone load cell was 700 Hz.[12]

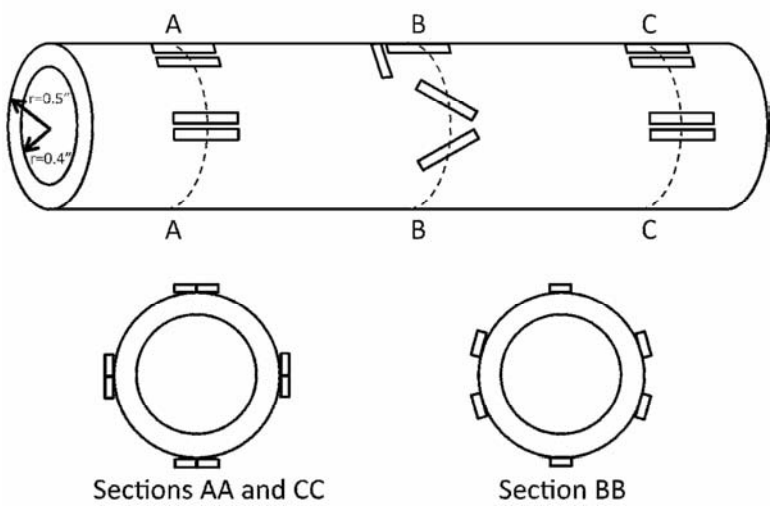

Figure 1. Diagram of strain gage configuration along walker handle.

The sensors consisted of a series of four-arm strain gage bridges. They were lightweight, with each load cell weighing about 100 grams. They were cylindrical, with a diameter of 38 millimeters and height of 60 millimeters. The load cells were tethered to two AMTI force plate amplifiers (model MSA-6) with 24-pin connector cables. Based on preliminary data analysis, the amplifier gains were set to 4000 for the vertical force channels, 2000 for the shear force channels, and 1000 for all of the moment channels.[12]

The instrumented handles were designed to be compatible with a variety of sizes and brands of walking frames, as well as anterior and posterior walker types. An anterior walker has a frame that is extended in front of the user, while a posterior walker's frame extends behind the user.

The instrumented walker handles, along with a unique biomechanical model, have been used to determine UE joint reaction forces and moments in healthy adults[10,13] and children with cerebral palsy.[11,12,14–17] This system is currently being used to test patients with cerebral palsy, OI, myelomeningocele, and spinal cord injury. This study presents internal joint

reaction force and moment data at the wrists, elbows and shoulders from one subject with OI and addresses the application of the system to the OI population.

METHODS

Kinematic Model

The UEs were modeled with seven rigid body segments: trunk, left and right upper arms, left and right forearms, and left and right hands). Sixteen passive reflective spherical markers were affixed to anatomical landmarks (Table 1, Figure 2) with double-sided tape and two were placed on the walker legs. Custom software was used for dynamic modeling.

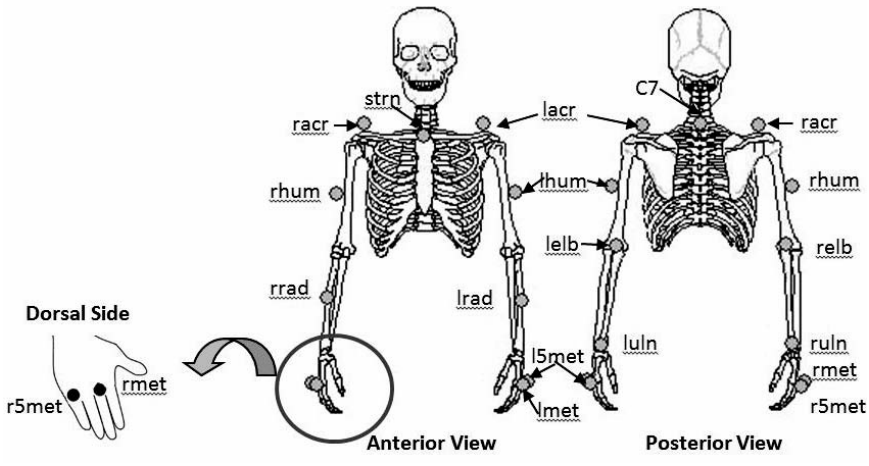

Figure 2. Marker configuration.

The body segment parameters used in this model were calculated based on Yeadon and Morlock's work in 1989.[18] Measurements of segment lengths and joint perimeters were used as inputs to equations used to calculate moments of inertia and masses of each segment. The center of gravity locations of each segment were calculated using equations from Chandler.[19] Although these equations were developed for adults, it has been shown that errors in body segment parameter estimations do not result in significant errors in the kinetic data.[20]

Table 1. Upper extremity (UE) marker locations.

Bony Landmark	Label	Marker Location
C7 vertebral process	C7	Most protruding vertebra on neck
Sternal notch	strn	Top of the sternum, between lowest part of the clavicles
Acromion process	lacr/racr	Top of shoulder
Mid-humerus	lhum/rhum	Mid-point of the lateral humerus
Olecranon	lelb/relb	Tip of the elbow
Radius	lrad/rrad	Mid-point of the radius
Ulnar styloid process	luln/ruln	Medial wrist bone
3rd metacarpal	lmet/rmet	Head of the middle finger
5th metacarpal	l5met/r5met	Head of the little finger

Segment Coordinate Systems

The current study reports the angles, forces, and moments in the reference system recommended by the International Society of Biomechanics (ISB). Positive x is anterior, positive y is superior, and positive z is directed laterally to the right. However, the model was developed under a different reference system convention in which positive x is anterior, positive y is directed laterally to the left and positive z is superior. A post-processing transformation was performed to allow the results to be reported in the ISB recommended system. The following description of the kinematic model will use the original reference system conventions.

Trunk

The trunk was modeled using the sternal notch, C7, and left and right anterior superior iliac spine (ASIS) markers from the LE marker set (Plug-In-Gait, Vicon, Oxford, UK). The z axis was defined using a vector from the pelvic center (midpoint between the ASIS markers) and the neck center (midpoint between the sternal notch and C7 markers). The y axis was defined by a vector from the left ASIS marker to the pelvic center. The x axis was the cross product of the y and z axes.

Upper Arm

The upper arm segments were modeled using the acromion process, mid-humerus, and olecranon markers. The origin was placed at the shoulder joint center (midpoint of the measured shoulder circumference). The z axis was defined using vectors connecting the shoulder joint center and the elbow joint center (midpoint of the elbow diameter). A temporary axis was constructed as a vector from the mid-humerus marker to the shoulder joint center. The x axis was defined as the cross product of the z axis and the temporary axis. The y axis was the cross product of the z and x axes.

Forearm

The forearm segments were modeled using the olecranon, mid-radius, and ulnar styloid process markers. The origin was placed at the elbow joint center. The z axis was defined as a vector from the wrist joint center (midpoint of the wrist diameter) to the elbow joint center. A temporary axis was constructed from the shoulder joint center to the elbow joint center. The y axis was defined as the cross product of the z axis and the temporary axis. The x axis was the cross product of the z and y axes.

Hand

The hand segments were modeled using the ulnar styloid process, third metacarpal and fifth metacarpal markers. The origin was placed at the wrist joint center. The z axis was defined as a vector from the third metacarpal joint to the wrist joint center. A temporary axis was constructed from the third metacarpal to the fifth metacarpal. The x axis was defined as the cross product of the z axis and the temporary axis. The y axis was the cross product of the z and x axes.

Rotation Sequence

The transformation matrix used to evaluate UE joint kinematics was computed using a sagittal-coronal-transverse rotation sequence, where α is the rotation in the sagittal plane, β is the rotation in the coronal plane, and γ is the rotation in the transverse plane (Equation 1).

$$[R] = \begin{bmatrix} \cos\alpha\cos\gamma + \sin\alpha\sin\beta\sin\gamma & \cos\beta\sin\gamma & -\sin\alpha\cos\gamma + \cos\alpha\sin\beta\sin\gamma \\ -\cos\alpha\sin\gamma + \sin\alpha\sin\beta\cos\gamma & \cos\beta\cos\gamma & \sin\alpha\sin\gamma + \cos\alpha\sin\beta\cos\gamma \\ \sin\alpha\cos\beta & -\sin\beta & \cos\alpha\cos\beta \end{bmatrix} \quad (1)$$

Angular velocities (ω_x, ω_y, ω_z) are given by Equation 2. Angular accelerations ($\dot{\omega}$) were calculated by taking the derivatives of the angular velocities.

$$\begin{aligned}\omega_x &= \dot{y}\sin(z)\cos(x) + \dot{x}\cos(z)\\ \omega_y &= \dot{y}\cos(z)\cos(x) - \dot{x}\sin(z)\\ \omega_z &= -\dot{y}\sin(x) + \dot{z}\end{aligned} \quad (2)$$

Kinetic Model

The kinetic calculations in this model follow the inverse dynamics equations based on the work of Vaughan and colleagues.[21] This method calculated the reaction force in the proximal joint ($\overline{F}_{\text{Joint}}$) using the mass-acceleration product (m = mass, $\bar{a}$ = acceleration, $\overline{g}$ = acceleration due to gravity) of the segment and the distal joint force contribution ($\overline{F}_{\text{Distal}}$), as shown in Equation 3. The rate of change of angular momentum ($\dot{H}$) is calculated using the mass moments of inertia (I_{XX}, I_{YY}, I_{ZZ}), angular velocities (ω_x, ω_y, ω_z), and angular accelerations ($\dot{\omega}_x$, $\dot{\omega}_y$, $\dot{\omega}_z$) as shown in Equation 4. The reaction moment in a joint of interest ($\overline{M}_{\text{Joint}}$) was calculated using the rate of change of angular momentum ($\dot{H}$) of the segment distal to it (Equation 4), the moment in the distal joint ($\overline{M}_{\text{Distal}}$), and the contributions of the forces ($\overline{F}_{\text{Proximal}}$, $\overline{F}_{\text{Distal}}$) crossed with the moment arms ($\bar{r}_{\text{proximal}}$, $\bar{r}_{\text{distal}}$) of the distal and proximal joints (Equation 5).[22]

$$\overline{F}_{\text{Joint}} = -m_{\text{DistalSegment}}(\bar{a}_{\text{DistalSegment}} + \bar{g}) + \overline{F}_{\text{Distal}} \quad (3)$$

$$\begin{aligned}\dot{H}_X &= I_{XX}\dot{\omega}_X - (I_{YY} - I_{ZZ})\,\omega_Z\,\omega_Y\\ \dot{H}_Y &= I_{YY}\dot{\omega}_Y - (I_{ZZ} - I_{XX})\,\omega_X\,\omega_Z\\ \dot{H}_Z &= I_{ZZ}\dot{\omega}_Z - (I_{XX} - I_{YY})\,\omega_Y\,\omega_X\end{aligned} \quad (4)$$

$$\overline{M}_{\text{Joint}} = \dot{H}_{\text{DistalSegment}} + \overline{M}_{\text{Distal}} - \left[\bar{r}_{\text{Proximal}} \times \overline{F}_{\text{Proximal}}\right] + \left[\bar{r}_{\text{Distal}} \times \overline{F}_{\text{Distal}}\right] \quad (5)$$

The most distal segment (hand) used the sensor outputs for $\overline{F}_{\text{Distal}}$ and $\overline{M}_{\text{Distal}}$. The center of mass of the hand was assumed to apply the load at the center of the handle. The distance from the center of the load cell to the center of the handle was factored in to the kinetic equations.

The axes were transformed to the ISB recommended system (x anterior, y superior, z lateral to the right). For the purposes of clinical reporting, adjustments were made to left side x and y angles so that adduction and internal rotation were positive for both left and right sides. Similarly, right side z forces were negated so that medial forces were always positive, and left side x and y moments were negated so that medial bending and internal rotation moments were always positive.

With these adjustments in mind, the following conventions apply to the results shown in this study. A positive joint reaction force (JRF) along the local y axis (superior) indicates compression of the joint. A positive JRF along the local x axis (anterior) indicates a posterior shearing force applied to the joint by the distal segment. A positive JRF along the z axis (medial) indicates a lateral shearing force applied to the joint by the distal segment. In a system with simplified force applications, pushing down on the walker handle would produce a superior (+y) JRF; pushing forward on the handle would produce a posterior (-x) JRF; and pushing outward on the handle would produce a medial (+z) JRF.[15]

The joint reaction moments (JRMs) reported with this model can be described in terms of the demands placed on the joints by the forces and moments applied to the joint. For example, a positive JRM about the segment's medial/lateral (z) axis indicates that there is a demand on the flexor muscles to keep the joint stable, while a negative JRM indicates a demand on the extensors. Moments about the anterior/posterior (x) axis describe the demands on the adductors and abductors, with abductors being positive. Finally, moments about the superior/inferior (y) axis describe the demands on the muscles that cause internal and external rotation, with internal rotation being positive.[23] These are similar to the conventions described in Winter et al.[24] See Table 2 for a summary of the coordinate system terminology and sign conventions.

Table 2. Coordinate system terminology.

Axis & Sense	Angle	Force	Moment
+x	Adduction	Anterior	Medial Bending
-x	Abduction	Posterior	Lateral Bending
+y	Internal Rotation	Superior	Internal Rotation
-y	External Rotation	Inferior	External Rotation
+z	Flexion	Medial	Flexion
-z	Extension	Lateral	Extension

The calculated joint reaction forces and moments were normalized in this study. The forces were divided by the subject's weight (N) to obtain a unitless "percent body weight" metric. This is a common method used by many researchers.[6,7,25] The moments were divided by the product of the subject's weight (N) and height (mm). This resulted in a unitless "percent body weight times height" metric. This method is also used elsewhere in literature; however some researchers only normalize moments to body weight.[25]

Subject Demonstration

After appropriate Institutional Review Board approval and subject consent and assent forms had been obtained, a subject (male, age: 15.5 years, weight: 27.7 kg, height: 1.19 m) with OI type III underwent gait testing. UE and LE body segment measurements were recorded. A standard lower body marker set (Plug-In-Gait) was applied to the LEs, and the custom UE marker set, described above, was applied to the upper body.

A pediatric walker (Sunrise Medical, Guardian Strider 07781, Longmont, CO) was fitted with handles instrumented with custom strain gage-based dynamometers (MCW-6-500, AMTI, Watertown, MA), described above (Figure 3). This type of walker was made of lightweight aluminum, had adjustable height legs, and could be used in the anterior or posterior configuration. The walker was used in the posterior configuration for this subject. The handle height was adjusted so that they reached the subject's ulnar styloid process when standing with arms relaxed, and the handle grips were positioned horizontally. A 14-camera motion analysis system (Vicon, Oxford Metrics, Oxford, UK), collecting data at 120 Hz, was used to capture the motion of the reflective markers in three dimensions. A Woltring filter with a mean-squared-error of 20 was applied to motion data.

A baseline trial with the unloaded walker alone was recorded. The force and moment values acquired from the baseline trial were used as an offset for the

motion trials. A static reference trial was collected with the subject standing in a comfortable position within the walker frame. This trial was used for marker labeling purposes. The subject then performed at least 10 walking trials, ensuring that at least 5 acceptable gait cycles were obtained. Three-dimensional load cell data was collected simultaneously at 1500 Hz.

Figure 3. Instrumented posterior walker.

RESULTS

Shoulder

The greatest forces seen at the shoulders were anterior shear forces. The left side saw greater forces (5.6 to 13.6 percent body weight (% BW)) than the right (4.8 to 11.8 % BW).

The greatest moments seen at the shoulders were flexion/extension moments. The left side experienced flexion moments ranging from 1.2 to 3.4 percent body weight times height (% BW*H). The right side experienced extension moments ranging from -1.6 to -3.3% BW*H. Shoulder angle, force, and moment plots are shown in Figure 4. Complete results are shown in Tables 3 and 4.

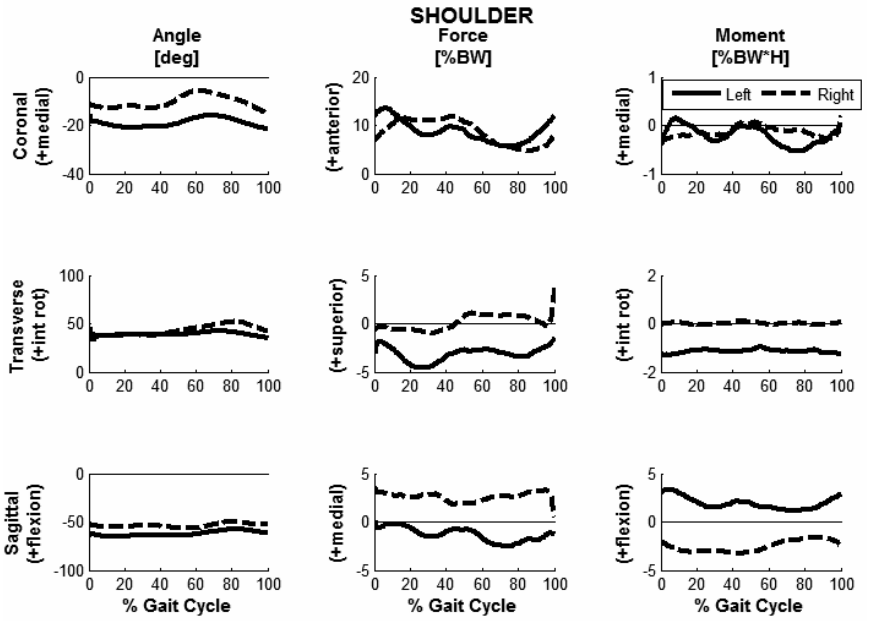

Figure 4. Bilateral shoulder (glenohumeral) joint angles, JRFs, and JRMs for a subject with OI in three planes.

Table 3. Joint reaction forces (%BW).

		Left			Right		
	(+/-)	min	max	range	min	max	range
Shoulder	M/L	-2.5	0.1	2.6	0.5	3.6	3.1
	S/I	-4.6	-1.4	3.2	-1.0	3.8	4.8
	A/P	5.6	13.6	8.0	4.8	11.8	7.0
Elbow	M/L	-1.9	1.2	3.1	4.3	7.9	3.6
	S/I	-9.6	-2.5	7.2	-5.8	-0.2	5.6
	A/P	-5.9	-3.9	2.0	-1.9	1.7	3.5
Wrist	M/L	3.3	5.6	2.3	-4.4	-2.3	2.2
	S/I	1.0	2.5	1.6	-0.9	0.9	1.8
	A/P	0.5	7.5	7.0	1.6	8.1	6.4

M/L = Medial/Lateral shear force, with medial being positive and lateral being negative.
S/I = Superior/Inferior force, with superior being positive and inferior being negative.
A/P = Anterior/Posterior shear force, with anterior being positive and posterior being negative.

Table 4. Joint reaction moments (%BW*H).

		Left			Right		
	(+/-)	min	max	range	min	max	range
Shoulder	M/L	1.2	3.4	2.3	-3.3	-1.6	1.7
	S/I	-1.3	-1.0	0.3	0.0	0.1	0.2
	A/P	-0.5	0.4	1.0	-0.4	0.2	0.6
Elbow	M/L	-0.5	0.0	0.5	-1.1	-0.9	0.2
	S/I	-0.3	0.0	0.3	0.0	0.1	0.1
	A/P	1.0	1.3	0.3	0.0	0.1	0.2
Wrist	M/L	1.0	1.8	0.8	0.8	1.7	0.8
	S/I	-0.7	-0.4	0.4	-0.3	-0.1	0.2
	A/P	0.4	0.7	0.3	0.2	0.4	0.2

F/E = Flexion/Extension moment, with flexion being positive and extension being negative.
I/E = Internal/External rotation moment, with internal rotation being positive and external rotation being negative.
M/L = Medial/Lateral bending moment, with medial bending being positive and lateral bending being negative.

Elbow

The greatest forces seen at the elbows were inferiorly directed forces. The left side saw greater forces (-2.5 to -9.6% BW) than the right side (-0.2 to -5.8% BW).

The greatest moments seen at the left elbow were medial bending moments (1.0 to 1.8% BW*H), while the greatest moments seen at the right elbow were extension moments (-0.9 to -1.1 %BW*H). Elbow angle, force, and moment plots are shown in Figure 5.

Wrist

The greatest forces seen at the wrists were anterior shear forces. The right side saw slightly greater forces (1.6 to 8.1% BW) than the left side (0.5 to 7.5% BW).

The greatest moments seen at the wrists were flexion moments. The left side experienced moments ranging from 1.0 to 1.8% BW*H, while the right side experienced moments ranging from 0.8 to 1.7% BW*H. Wrist angle, force, and moment plots are shown in Figure 6.

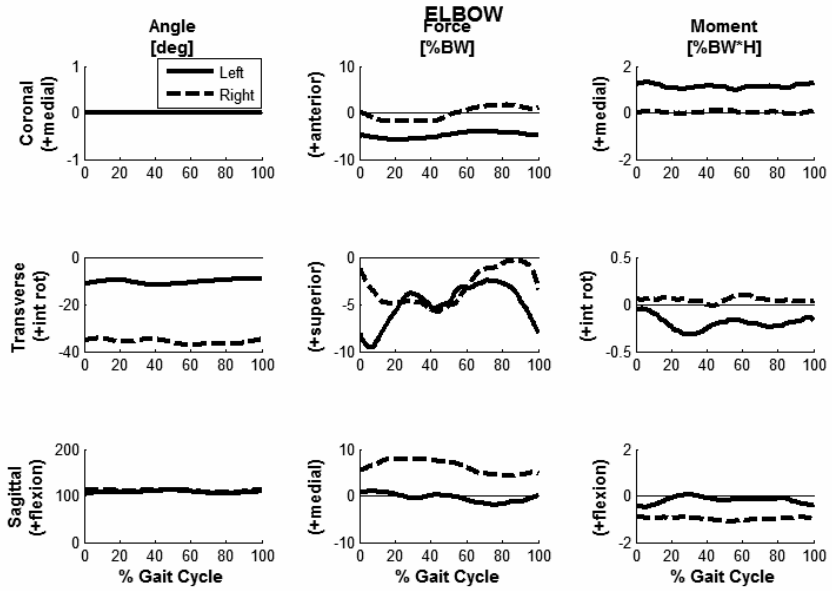

Figure 5. Bilateral elbow joint angles, JRFs, and JRMs for a subject with OI in three planes.

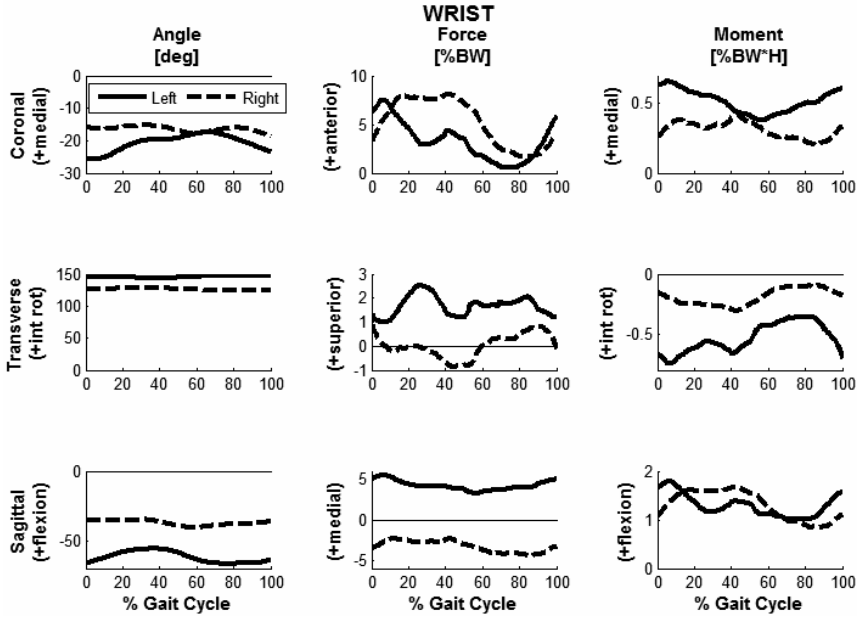

Figure 6. Bilateral wrist joint angles, JRFs, and JRMs for a subject with OI in three planes.

DISCUSSION

No previous studies have examined the UE dynamics during walker-assisted gait in the OI population. The results from the single subject analyzed here are not directly comparable to other studies, and there is no normal walker user population since all walker users have pathology. However, the general magnitudes and patterns can be compared and contrasted to other pediatric walker users. Our group has completed a study examining the JRFs and JRMs of 10 children with cerebral palsy (CP) during anterior and posterior walker use.[15] This study showed the greatest JRFs in the superior direction at the wrist (up to 6% BW), elbow (up to 7% BW), and shoulder (up to 4% BW). The current study shows the greatest JRFs in the shoulder and wrist to be anterior shear forces (up to 13.6% BW in the left shoulder; up to 8.1% BW in the right wrist). Anterior shear JRFs occur due to the extended posture of the shoulders throughout the gait cycle. The left elbow experienced inferior JRFs up to -9.6% BW. The CP study shows that the greatest JRMs occur in the shoulder (1.1% BW*H flexion). The current study also shows the greatest JRMs occurring in the shoulder joints, with left shoulder flexion moments up to 3.4% BW*H and right shoulder extension moments up to -3.3% BW*H.

The current results show generally higher absolute JRFs and JRMs than the CP study, however the results are reasonable. The CP study is an average of 10 subjects. Averaging data has the effect of attenuating peaks, which could account for the lower magnitude of the maximum and minimum values seen there. Other differences could be due to pathology, walking style and speed, and specific motion patterns exhibited by the current subject.

The results show several differences bilaterally. For example, the left shoulder experienced inferior JRFs and flexion JRMs over the entire gait cycle, while the right shoulder experienced mostly superior JRFs and all extension JRMs. This is not uncommon when dealing with pathology that affects each limb differently. The subject may favor one side due to pain, or experience musculoskeletal constraints that do not allow bilateral symmetry. Because of these differences, it is imperative that each side be examined separately, as with this instrumented walker system.

According to Wolff's law, bone adapts to the loads placed on it. Increase in load causes the trabeculae to undergo adaptive changes, followed by secondary changes to the cortical bone, making the bone denser and stronger. The converse is also true: decreased loading on a bone results in decreased bone density and therefore decreased strength and increased

fracture risk.[26] Therefore, it is important for children with OI to remain active, but it is also essential to monitor their activity to reduce fracture risk. Walking aids put added loads on the UEs, while relieving loads from the LEs. The lowered loading conditions on the LEs could mitigate fracture risk in the legs, and the increased loads on the UEs could help to maintain or even increase the strength of the UE bones. However, long-term walking aid use has been shown to have negative effects on the UE joints and soft tissue, including arthritis, shoulder rotator cuff injury, and carpal tunnel syndrome.[27,28] More research is needed to determine the optimal loading conditions to keep the bone healthy while also avoiding UE injury during aided ambulation.

We conclude that the instrumented walker system and UE model described here are useful for quantifying and analyzing UE kinematics and kinetics during walker-assisted gait in children with OI. The ability to evaluate and monitor the loads placed on the UE joints could be useful in decreasing the risk of UE injury through improved therapy and walking aid modifications.

ACKNOWLEDGEMENTS

We would like to acknowledge James Van Bogart, Jason Long, Kathy Reiners and Sahar Hassani for their role in patient selection, scheduling, and testing at the Medical College of Wisconsin and Shriner's Hospital, Chicago.

ABBREVIATIONS

ASIS	Anterior superior iliac spine
CP	Cerebral palsy
C7	7th cervical vertebra
ISB	International society of biomechanics
JRF	Joint reaction force
JRM	Joint reaction moment
LE	Lower extremity
OI	Osteogenesis imperfecta
UE	Upper extremity
%BW	Percent body weight
%BW*H	Percent body weight times height

REFERENCES

1. Freemont A. The pathology of osteogenesis imperfecta. *J. Clin. Pathol.* 1996;49(8):618-619.

2. Marini JC. Osteogenesis imperfecta. In: *Nelson Textbook of Pediatrics*. 19th ed. Philadelphia, PA: Saunders Elsevier; 2011:692.
3. Wu G, van der Helm FCT, Veeger HEJD, et al. ISB recommendation on definitions of joint coordinate systems of various joints for the reporting of human joint motion--Part II: shoulder, elbow, wrist and hand. *J Biomech*. 2005;38(5):981-992.
4. Fast A, Wang FS, Adrezin RS, et al. The instrumented walker: usage patterns and forces. *Arch Phys Med Rehabil*. 1995;76(5):484-491.
5. Finkel J, Fernie G, Cleghorn W. A guideline for the design of a four-wheeled walker. *Assist Technol*. 1997;9(2):116-129.
6. Melis EH, Torres-Moreno R, Barbeau H, Lemaire ED. Analysis of assisted-gait characteristics in persons with incomplete spinal cord injury. *Spinal Cord*. 1999;37(6):430-439.
7. Opila KA, Nicol AC, Paul JP. Forces and impulses during aided gait. *Arch Phys Med Rehabil*. 1987;68(10):715-722.
8. Pardo RD, Deathe AB, Winter DA. Walker user risk index. A method for quantifying stability in walker users. *Am J Phys Med Rehabil*. 1993;72(5):301-305.
9. Bachschmidt R, Harris G, Simoneau G. Development of an instrumented walker for measurement of unilateral hand loads. In: *Proceedings of the 1996 Fifteenth Southern Biomedical Engineering Conference*. Dayton, OH: Institute of Electrical and Electronics Engineers; 1996.
10. Bachschmidt RA, Harris GF, Simoneau GG. Walker-assisted gait in rehabilitation: a study of biomechanics and instrumentation. *IEEE Trans Neural Syst Rehabil Eng*. 2001;9(1):96-105.
11. Bachschmidt RA, Harris GF, Ackman J, et al. Development of a system for quantitative study of pediatric walker-assisted gait. In: *Proceedings of the 20th Annual Internation Conference of the IEEE Engineering in Medicine and Biology Society*.Vol 20(5). IEEE; 1998:2689-2692.
12. Bachschmidt RA, Harris GF. Quantitative Study of Walker-Assisted Gait in Children with Cerebral Palsy: Anterior versus Posterior Walkers. In: *Pediatric Gait: A New Millenium in Clinical Care and Motion Analysis Technology*. Piscataway, NJ: IEEE Press; 2000:217.
13. Simoneau GG, Hambrook G, Bachschmidt RA, Harris GF. Quantifying upper extremity efforts when using a walking frame. In: *Pediatric Gait: A New Millenium in Clinical Care and Motion Analysis Technology*. Piscataway, NJ: Institute of Electrical Engineers, Inc. 2000:210.
14. Baker KM, Wang M, Cao K, et al. Biomechanical System for the Evaluation of Walker-Assisted Gait in Children: Design and Preliminary Application. In: *Proceedings of the 25th Annual International Conference of the IEEE EMBS*. Cancun, Mexico; 2003:1851-1854.
15. Konop KA, Strifling KMB, Wang M, et al. A biomechanical analysis of upper extremity kinetics in children with cerebral palsy using anterior and posterior walkers. *Gait Posture*. 2009;30(3):364-369.
16. Konop KA, Strifling KMB, Wang M, et al. [Upper extremity kinetics and energy expenditure during walker-assisted gait in children with cerebral palsy]. *Acta Orthop Traumatol Turc*. 2009;43(2):156-164.
17. Konop KA, Strifling KMB, Krzak J, Graf A, Harris GF. Upper Extremity Joint Dynamics During Walker Assisted Gait: A Quantitative Approach Towards Rehabilitative Intervention. *Journal of Experimental & Clinical Medicine*. 2011;3(5):213-217.

18. Yeadon MR, Morlock M. The appropriate use of regression equations for the estimation of segmental inertia parameters. *J Biomech*. 1989;22(6-7):683-689.
19. Chandler FR. *Investigation of inertial properties of the human body*. Wright Patterson Air Force Base, OH: Army Medical Research Lab; 1975.
20. Bauer JJ, Pavol MJ, Snow CM, Hayes WC. MRI-derived body segment parameters of children differ from age-based estimates derived using photogrammetry. *J Biomech*. 2007;40(13):2904-2910.
21. Vaughan C, Davis B, O'Connor J. *Dynamics of Human Gait*. Champaign, IL: Human Kinetics Press; 1992.
22. Strifling. Anaylsis and modeling of upper and lower extremity dynamics in children with cerebral palsy using walkers. 2006.
23. Konop KA. A biomechanical analysis of upper extremity kinetics in children with cerebral palsy using anterior and posterior walkers. 2008.
24. Winter. *Biomechanics and motor control of human movement*. 3rd ed. Hoboken, NJ: John Wiley & Sons, Inc. 2005.
25. Ounpuu S, Davis RB, DeLuca PA. Joint kinetics: Methods, interpretation and treatment decision-making in children with cerebral palsy and myelomeningocele. *Gait*. 1996;4:62-78.
26. Wolff J. The Classic: On the Inner Architecture of Bones and its Importance for Bone Growth. *Clinical Orthopaedics and Related Research*®. 2010;468(4):1056-1065.
27. Kellner WS, Felsenthal G, Anderson JM, Hilton EB, Mondell DL. Carpal tunnel syndrome in the nonparetic hands of hemiplegics. Stress-induced by ambulatory assistive devices. *Orthop Rev*. 1986;15(9):608-611.
28. Klimaitis A, Carroll G, Owen E. Rapidly progressive destructive arthropathy of the shoulder--a viewpoint on pathogenesis. *J. Rheumatol.* 1988;15(12):1859-1862.